

Structural properties of $\text{Sr}_{0.61}\text{Ba}_{0.39}\text{Nb}_2\text{O}_6$ in the temperature range 10–500 K investigated by high-resolution neutron powder diffraction and specific heat measurements

J. Schefer,¹ D. Schaniel,² V. Pomjakushin,¹ U. Stuhr,¹ V. Petříček,³ Th. Woike,² M. Wöhlecke,⁴ and M. Imlau^{4,*}

¹Laboratory for Neutron Scattering, ETH & PSI, CH-5232 Villigen, PSI, Switzerland

²Institut für Mineralogie, University at Cologne, D-50674 Köln, Germany

³Institute of Physics, Academy of Sciences of the Czech Republic, Na Slovance 2, 18221 Praha 8, Czech Republic

⁴Fachbereich Physik, University of Osnabrück, D-49069 Osnabrück, Germany

(Received 1 June 2006; published 3 October 2006)

We report high-resolution neutron powder diffraction on $\text{Sr}_{0.61}\text{Ba}_{0.39}\text{Nb}_2\text{O}_6$ in the temperature range 15–500 K. The results indicate that the low-temperature anomalies ($T \leq 100$ K) observed in the dielectric dispersion are due to small changes in the incommensurate modulation of the NbO_6 octahedra, as no structural phase transition of the average structure was observed. This interpretation is supported by specific heat measurements, which show no latent heat, but a glass-like behavior at low temperatures. Furthermore, we find that the structural changes connected with the ferroelectric phase transition at $T_c \approx 350$ K start already at 200 K, explaining the anisotropic thermal expansion in the temperature range 200–300 K observed in a recent x-ray diffraction study.

DOI: [10.1103/PhysRevB.74.134103](https://doi.org/10.1103/PhysRevB.74.134103)

PACS number(s): 61.12.Ld, 33.15.Dj

I. INTRODUCTION

Strontium barium niobate ($\text{Sr}_x\text{Ba}_{1-x}\text{Nb}_2\text{O}_6$, SBN_x) exhibits very large electro-optic, piezoelectric, and pyroelectric coefficients^{1,2} and is therefore of significant interest for a variety of applications, especially as a photorefractive material with a high two-beam coupling coefficient Γ .^{2,3} Furthermore, SBN is a model substance for the investigation of the relaxor-type ferroelectric phase transition, where ferroelectric nanoclusters are stabilized by internal random fields above the critical temperature T_c over a wide temperature range, such that the ferroelectric polarization does not decay spontaneously at T_c .⁴ This relaxor behavior is well explained by the random-field Ising model for the ferroelectric phase transition. Assuming an internal random electric field, all critical exponents could be determined according to the scaling relation.^{5–7} They satisfy the Rushbrooke relation and belong to the universal class of the three-dimensional Random-field Ising model. During this high-temperature ferroelectric phase transition the space group of the average structure changes from $P-4b2$ to $P4bm$, while the incommensurate modulation remains.^{8,9}

SBN belongs to the large class of materials with open tungsten bronze structure. This structure is characterized by a network of NbO_6 octahedra, which are connected by the edges to form pentagonal A2, tetragonal A1, and trigonal C channels (see Fig. 1). The 12-fold-coordinated A1 position is occupied only by Sr, while the 15-fold-coordinated A2 site is shared between Sr and Ba. The C positions remain empty. Since only five Sr or Ba atoms are occupying the 6A1 and A2 sites, one of the A1 and A2 sites remains empty. The incommensurate structure¹⁰ is due to a tilting of the oxygen octahedra with respect to the c axis. Neglecting the incommensurate nature of the modulation, this bending was earlier described by two configurations for the oxygen octahedra.¹¹

There is an ongoing discussion about a second phase transition at temperatures below 100 K.^{12–16} Based on dielectric, pyroelectric, and structure measurements, a phase transition

from the tetragonal (4 mm) phase into an orthorhombic or monoclinic (m) phase was postulated.¹² This postulation is supported by temperature-dependent dielectric and pyroelectric signals in the [100] and [110] directions, which are forbidden in the tetragonal 4 mm point group. On the other hand, in an early x-ray powder diffraction study¹³ only small changes in the lattice parameters a and c were detected, without indications for a phase transition into a monoclinic phase. Later, Ko *et al.*¹⁴ confirmed the dielectric measurements, but argued that the signals are not necessarily due to a structural phase transition, but might as well be due to a temperature-driven charge or polaronic hopping process, or even a temperature-driven flipping process of the oxygen octahedra, which should be reflected in the incommensurate

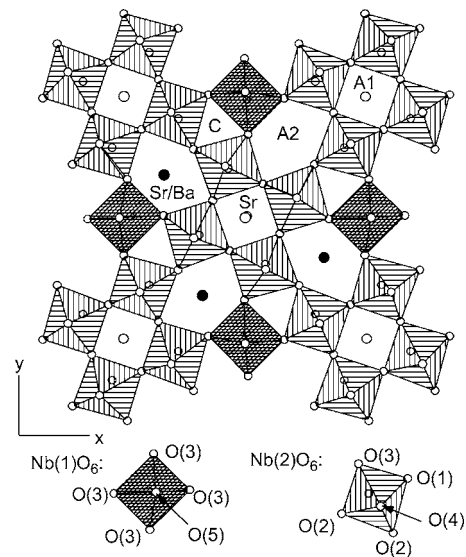


FIG. 1. Projection of $\text{Sr}_{0.61}\text{Ba}_{0.39}\text{Nb}_2\text{O}_6$ along the c axis. The pentagonal channels A2 are filled by Sr or Ba, the tetragonal channels A1 by Sr, and the trigonal channels C remain empty. Five Sr and/or Ba atoms are distributed over six A1 and A2 sites.

positions of the oxygen atoms. The activation energy for this process was given as 0.087 eV. More recent evidence for a structural phase transition was claimed from Raman spectroscopy,¹⁵ while a subsequent ir study gave no clear evidence for a new phase transition below 100 K.¹⁶

In order to clarify whether the observed dielectric anomalies below 100 K are due to a structural phase transition, we performed temperature-dependent neutron diffraction experiments on powders of SBN61, and specific heat measurements on single crystals of SBN61. Neutron diffraction offers the advantage of a high sensitivity to oxygen and hence allows for a detailed investigation of the influence of the NbO₆ octahedra on the observed physical properties. The neutron diffraction experiments were carried out in the temperature range 15–500 K, while the specific heat was recorded from 2 to 300 K. We could not observe signatures of a structural phase transition, which supports the interpretation of Ko *et al.*¹⁴ that a dynamical process, like the concerted rotation of the oxygen octahedra, is at the origin of the observed phenomena.

II. EXPERIMENTAL DETAILS

The congruent SBN61 crystals were grown by the Czochralski method in the crystal growth laboratory of the University of Osnabrück. The polycrystalline sample was produced by grinding a single crystal.

Specific heat measurements were performed in the temperature range 2–300 K by the relaxation method using a physical property measurement system (PPMS) from Quantum Design. Good thermal contact between the single-crystal sample and the sapphire chip of the system was made with Apiezon grease.

The neutron powder diffraction experiments were performed on the high-resolution powder diffractometer¹⁷ HRPT at the Swiss Spallation Neutron Source (SINQ),¹⁸ using $\lambda = 1.886$ Å. Temperature-dependent measurements were done in the high-intensity mode. Additionally, two patterns at $T = 15$ and 290 K have been recorded using the high-resolution mode (primary collimation $\alpha_1 = 12$) on HRPT. In order to determine the lattice constants with high accuracy further powder diffraction experiments were performed on the high-resolution neutron strain scanner¹⁹ POLDI in the temperature range 300–500 K. A chopper running at 10 000 rpm allows for the analysis of the frame-overlapping time-of-flight data. Apart from the (620) and (002) reflections, we analyzed only fully separated reflections in order to get the highest accuracy. The concept of the instrument is described in detail by Stühr.²⁰

III. RESULTS

A. Specific heat

The specific heat of SBN61 was measured in the temperature range 2–300 K (Fig. 2). No latent heat was observed in this temperature range. The data were analyzed using the well-known Debye relation and three Einstein oscillators, such that

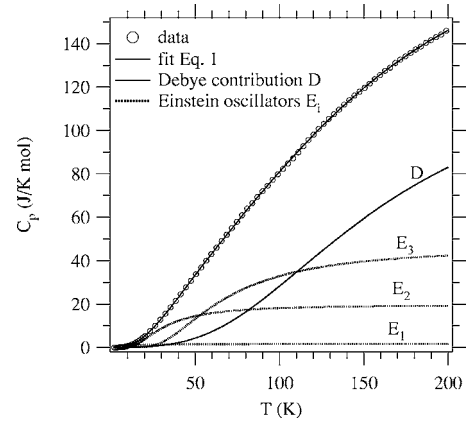


FIG. 2. Specific heat in the temperature range 2–200 K for Sr_{0.61}Ba_{0.39}Nb₂O₆. The solid line is a fit using Eq. (1); the dashed and dash-dotted lines correspond to the Einstein and Debye contributions, respectively.

$$C_p = 9n_D N_A k_B \left(\frac{T}{\theta_D} \right)^3 \int_0^{x_D} dx \frac{x^4 e^x}{(e^x - 1)^2} + 3N_A k_B \sum_{i=1}^3 n(E_i) \times \left(\frac{E_i}{T} \right)^2 \frac{e^{E_i/T}}{(e^{E_i/T} - 1)^2}, \quad (1)$$

where $x_D = \theta_D/T = \hbar\omega_D/k_B T$ with θ_D the Debye temperature, k_B the Boltzmann constant, N_A the Avogadro number, and ω_D the Debye frequency. The parameter n_D denotes the relative strength of the Debye contribution, $n(E_i)$ that of the single Einstein oscillators, and E_i is the energy of the Einstein oscillators. Three Einstein oscillators were necessary since a fit with only two was not accurate in the low-temperature part. The fit is performed up to 200 K, since the structural data show that above this temperature the relaxor phase transition sets in (see below). From Fig. 2 it becomes clear that the Debye contribution is dominant above about 110 K; below that the Einstein oscillators are mainly contributing to the total specific heat. The contributions of the three Einstein oscillators are more clearly visible in Fig. 3, where the spe-

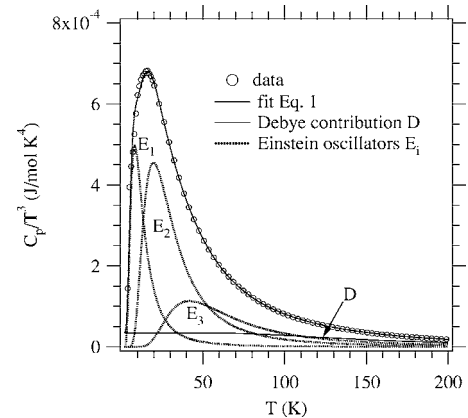


FIG. 3. Specific heat C_p/T^3 in the temperature range 2–200 K for Sr_{0.61}Ba_{0.39}Nb₂O₆. The solid line is a fit using Eq. (1); the dashed and dash-dotted lines correspond to the Einstein and Debye contributions, respectively.

TABLE I. Parameters of Einstein oscillators and Debye contribution obtained from a fit of Eq. (1) to the specific heat data in the temperature range 2–200 K.

i	E_i (K)	ν_i (cm^{-1})	$n(E_i)$
1	41(19)	29(12)	0.06 (8)
2	97(13)	67(10)	0.78(12)
3	206(11)	143(9)	1.85(12)
	θ_D (K)	ω_D (cm^{-1})	n_D
	681(8)	474(6)	5.6(1)

specific heat is plotted as C_p/T^3 versus T . The fit parameters are given in Table I.

B. Neutron diffraction: Temperature dependence

In order to detect a possible low-temperature structural phase transition we collected neutron diffraction powder patterns on HRPT between 10 and 300 K in the high-intensity mode. Figure 4 shows the low-angle part of these patterns, indicating that no structural phase transition takes place. In addition we collected two data sets in the high-resolution mode at 15 and 290 K. Also here no indication for a structural change was observed. Lattice parameters were determined from these powder patterns using the average structure $P4bm$. The volume of the tetragonal unit cell is steadily increasing below 300 K, as illustrated in Fig. 5. Between 300 and 400 K the high-temperature ferroelectric phase transition is clearly seen from the change in the lattice constant c as illustrated in Fig. 6. Fitting a polynomial $V(T) = V_0 + \alpha_V T + \beta_V T^2$ to the measured data below 300 K yields the parameters $\alpha_V = 3.7(3) \times 10^{-3} \text{ \AA}^3 \text{ K}^{-1}$, $\beta_V = 1.37(9) \times 10^{-5} \text{ \AA}^3 \text{ K}^{-2}$, and the volume $V_0 = V(T=0) = 608.65(2) \text{ \AA}^3$. The lattice constant a follows the same tendency, whereas the tetragonal c axis is decreasing for $T > 200$ K (see Fig. 6). In order to follow the change of the lattice parameters through the ferroelectric phase transition ($T_c \approx 350$ K) we performed further

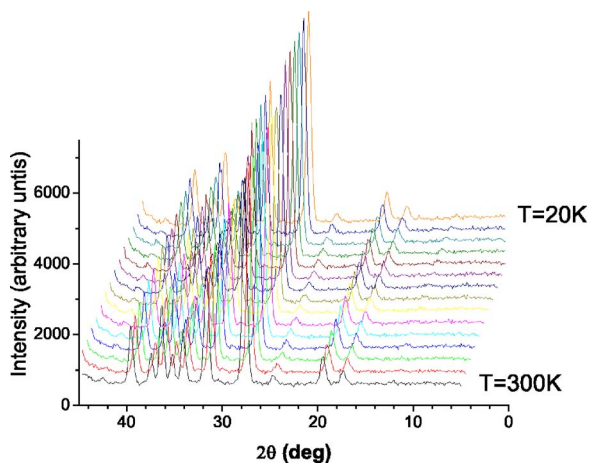


FIG. 4. (Color online) Section of the neutron diffraction patterns of SBN61 collected on HRPT using the high-intensity mode, $\lambda = 1.886 \text{ \AA}$, for $T = 300$ down to 20 K in steps of 20 K.

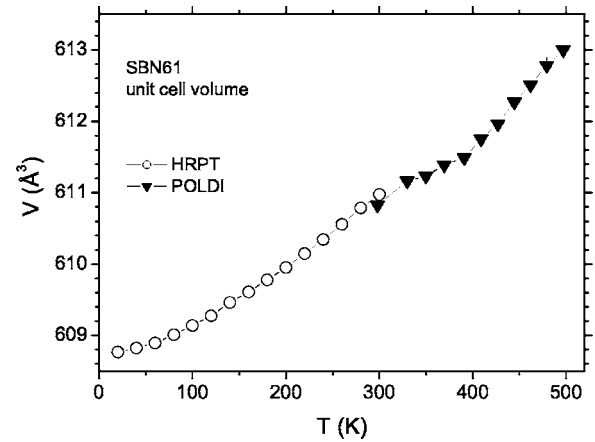


FIG. 5. Volume of the tetragonal unit cell in SBN61 as a function of temperature. Open circles correspond to HRPT data and closed triangles to POLDI data.

experiments on POLDI in the temperature range 300–500 K. Here the lattice parameters are obtained with high accuracy from separated reflections, as illustrated in Fig. 7 for the (620) and (002) reflections. In the ferroelectric $P4bm$ phase the two reflections accidentally overlap. As a result of the different temperature dependences of the a and c parameters in the high-temperature range they are split. Note that in Figs. 5 and 6 the lattice parameters obtained from the two different instruments were not corrected for the calibration difference of 0.1%. In total the lattice constant a shows the usual temperature dependence as it increases steadily below 300 K and changes its slope above 300 K. A polynomial fit $a(T) = a_0 + \alpha_a T + \beta_a T^2$ up to 300 K yields the parameters $\alpha_a = 1.0(4) \times 10^{-5} \text{ \AA K}^{-1}$, $\beta_a = 2.4(1) \times 10^{-7} \text{ \AA K}^{-2}$, and $a_0 = 12.4340(2) \text{ \AA}$. The lattice constant c , on the other hand, increases in a similar manner up to about 150 K, where a flattening sets in. Above about 200 K up to 400 K c decreases, and above 400 K it increases again. There is an indication for a second decrease above 500 K, but further measurements at higher temperatures are necessary to confirm this observation, which also has been observed in SBN82.²¹

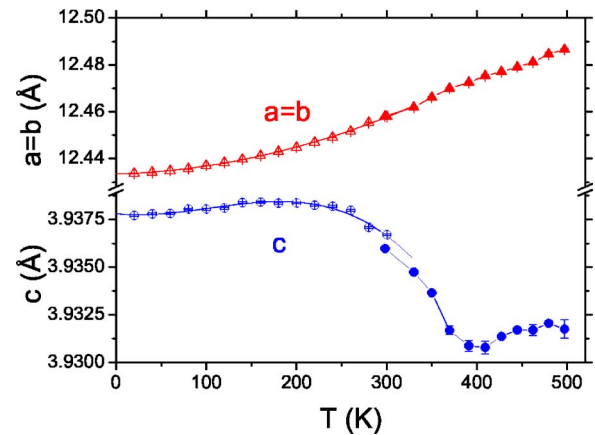


FIG. 6. (Color online) Tetragonal lattice constants a and c of SBN61 as a function of temperature. Open circles correspond to HRPT data ($T \leq 300$ K) and closed circles to POLDI data ($T \geq 300$ K).

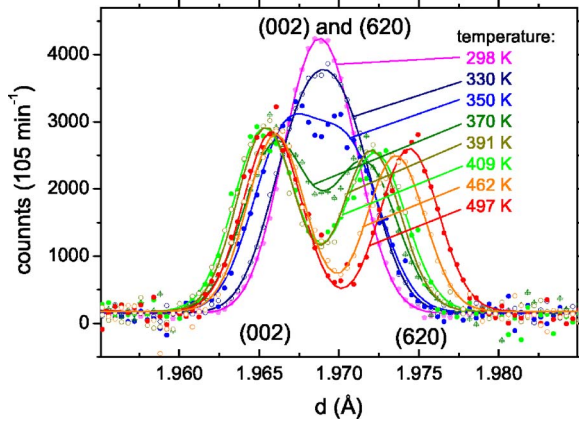


FIG. 7. (Color online) Splitting of the (620) and (002) reflections in $\text{Sr}_{0.61}\text{Ba}_{0.39}\text{Nb}_2\text{O}_6$, SBN61, observed with the high-resolution strain scanner POLDI (Ref. 19). At low temperatures, the two reflections nearly coincide, but split at higher temperatures as a result of the opposite temperature dependence of $a=b$ and c .

C. Neutron diffraction: Structural refinement

There is no direct evidence for a low-temperature structural phase transition from the tetragonal into an orthorhombic or monoclinic phase from the above presented data. In order to detect more subtle structural changes we investigated the two high-resolution powder patterns measured at 15 and 290 K in more detail. For this purpose we have to take into account that SBN61 has an incommensurately modulated structure, as was determined by single-crystal x-ray¹⁰ and neutron^{22,23} diffraction. However, the satellite peaks are too weak and too broad and hence cannot be separated in the powder patterns. Therefore we performed the refinement in three steps. First, the refinement was performed in the average structure, i.e., space group $P4bm$ without any modulation (model I). Second, we introduced a positional modulation for all atoms (model II), i.e., two harmonic waves were included to describe the positional modulation of each atom according to the two modulation vectors \mathbf{q}_1 and \mathbf{q}_2 . In the third step (model III) model II was extended with an additional modulation of the anisotropic displacement parameters (ADPs) on sites Sr2 and Ba. The refinement of the modulated structure has been done in five-dimensional space in space group $P4bm(pp1/2, pp1/2)$.²⁴ This elegant way to handle incommensurate structures by higher-dimensional space is integrated in JANA2000.²⁵ It is based on an extension of the standard formalism for reciprocal space to higher dimensions, including the incommensurate vectors (in our case, \mathbf{q}_1 and \mathbf{q}_2 yielding a five-dimensional space):

$$\mathbf{A}_i \cdot \mathbf{A}_j^* = \delta_{ij}, \quad i, j = 1 - 3, 4, 5, \quad (2)$$

where

$$\mathbf{A}_4^* = \mathbf{e}_1 + \mathbf{q}_1 \quad (3)$$

and

$$\mathbf{A}_5^* = \mathbf{e}_2 + \mathbf{q}_2 \quad (4)$$

with \mathbf{e}_1 and \mathbf{e}_2 perpendicular to real (reciprocal) space \mathfrak{R} .

The modulation vectors \mathbf{q}_1 and \mathbf{q}_2 have been fixed to $(0.3075, \pm 0.3075, 0)$ as determined from x-ray diffraction.¹⁰ A refinement of the \mathbf{q} directions is not possible as the satellites are too weak and too broad in the powder pattern. The occupation of the Ba site has been fixed to the known composition of 0.39 in all models and the sum of Ba and Sr atoms is fixed to 1. The results of the Rietveld refinements are summarized in Table II and given in detail in Tables V–VIII and Figs. 12 and 13 in Ref. 26. The quality of the refinements are illustrated in Figs. 8–10.

Figure 8 shows the refined pattern at 15 K after final refinement with model I, i.e., the average structure. There are no additional peaks or splittings indicating another space group or phase. However, the refinement is not satisfactory, as the peak intensities do not match very well. This is reflected also in the relatively high final χ^2 of 51.11 and 24.84 for the low- and high-temperature data, respectively (see Table II, columns 1 and 4) and the overestimated background in the region $2\theta \sim 42^\circ$ in Fig. 8. The fit quality is significantly better for the high-temperature data with $\chi^2=24.84$ compared to $\chi^2=51.11$ for the low-temperature data. The only significant differences in the refined parameters for the two data sets are observed in the x and y coordinates of the O4 atom, which change from $(0.0814(3), 0.2031(3), 0.221(2))$ at 290 K to $(0.0830(4), 0.2017(3), 0.217(2))$ at 15 K. Furthermore we note that the thermal displacement parameters of the O(4) and O(5) do not decrease with decreasing temperature and that the Sr(1) occupation is 0.65(1) and the Sr(2) occupation is 0.44(1). The parameters of the structural refinement of the average structure at 15 K and 290 K are listed in Table III.

Introducing positional modulation waves for all atoms significantly improves the refinement as illustrated in Figs. 9 and 10. The R values decrease to $R_{obs}=2.91$ and 2.93 for the low- and high-temperature data, respectively. Also the fit quality is improved, as now $\chi^2=22.27$ for the low-temperature data and 12.54 for the high-temperature data. The relative improvement is bigger for the low-temperature data (see Table II, column 2), but again the quality of the fit is better for the high-temperature data set. Motivated by this

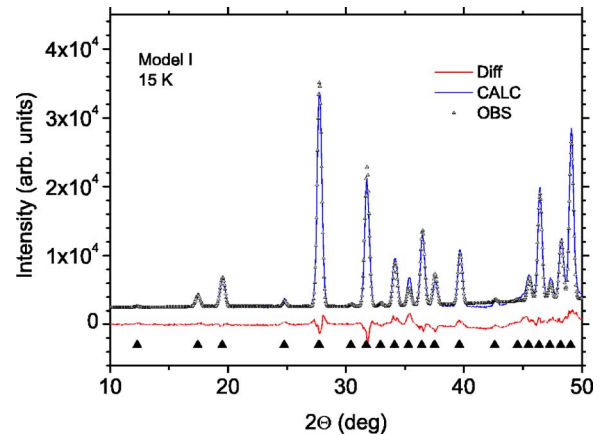


FIG. 8. (Color online) Section of the graphical result of the Rietveld refinement (Ref. 25) of the average structure (model I) of SBN61 powder data collected on HRPT using the high-resolution mode, $\lambda=1.886 \text{ \AA}$, at $T=15 \text{ K}$ (column 1, Table II).

TABLE II. Comparison of different refinements for Sr_{0.61}Ba_{0.39}Nb₂O₆ (SBN61) measured on HRPT at SINQ at $\lambda=1.886$ Å in the high-resolution mode. Tetragonal space group $P4bm/X4bm$ (no. 100) (Ref. 33), $Z=8$, $\mathbf{q}_{1,2}=(0.3075, \pm 0.3075, 0)$ (Ref. 10). Atoms are located on sites $2b$ (Nb1), $8d$ (Nb2), $2a$ (Sr1), $4c$ (Sr2, Ba@Sr2), $4c$ (O1), $8d$ (O2, O3, O4), and $2b$ (O5). The c axis of the incommensurate five-dimensional space group $X4bm$ is doubled compared to that of $P4bm$ in order to account for modulation along c with $q_z=0.5$. Structure refinement used JANA2000 (Ref. 25). Detailed results of the refinements using a positional modulated structure are given in Tables V–XII in the supplementary material (Ref. 26).

T (K)	15	15	15	290	290	290
Model	I	II	III	I	II	III
Positional modulation	Averaged	All sites	All sites	Averaged	All sites	All sites
ADP modulation		No	Site Sr2/Ba		No	Site Sr2/Ba
a (Å)	12.4387(3)	12.4383(2)	12.4383(2)	12.4626(3)	12.4619(2)	12.4620(2)
$c'=2c$ (Å)	7.8789(3)	7.8787(2)	7.8788(2)	7.8773(2)	7.8772(2)	7.8772(2)
$2 \times$ volume (Å ³)	1219.05(6)	1218.96(4)	1218.96(4)	1223.48(5)	1223.31(4)	1223.34(4)
χ^2	51.11	22.27	21.76	24.84	12.54	12.19
Main reflections						
R_{obs}	7.34	2.91	2.83	6.62	2.93	2.88
$R_{w,obs}$	5.42	2.61	2.57	4.99	2.66	2.61
R_{all}	7.28	2.91	2.83	6.69	2.93	2.88
$R_{w,all}$	5.42	2.61	2.57	4.99	2.66	2.61
n_{obs}	237	238	238	236	238	238
n_{all}	238	238	238	238	238	238
Satellites of order 1						
R_{obs}		4.53	4.49		4.82	4.64
$R_{w,obs}$		3.02	2.95		3.00	2.87
R_{all}		4.89	4.81		5.03	4.95
$R_{w,all}$		3.02	2.95		3.00	2.87
n_{obs}		765	767		768	768
n_{all}		777	777		779	779

success we included an additional modulation of the ADPs at the Sr2 and Ba sites, as this proved valuable in the single-crystal refinement.¹⁰ However, as can be seen from Table II (column 3), the improvement over model II is marginal, and is not significant. We thus concentrate on the results of model II for the comparison of the two structures at 15 and 290 K.

Before comparing the differences in the modulation parameters at $T=15$ and 290 K we wish to stress again that the description of the powder data with a modulated structure is feasible and necessary, although no separate satellite reflections could be measured. This is illustrated in Fig. 11, which shows observed Fourier maps for the atom O4 and the refined positional modulation as a function of the coordinate x_4 corresponding to the first modulation vector \mathbf{q}_1 . The atom O4 is lying in the plane of the Sr and Ba atoms, which occupy the A_1 and A_2 channels in the unfilled tungsten bronze structure (see Fig. 1). Due to the incomplete filling and disorder of Sr and Ba in these channels, the adjacent oxygen octahedra are tilted, leading to the observed incommensurate modulation.^{10,23} For the O4 atoms this results mainly in a positional modulation in the a - b plane (coordinates x, y). Figure. 11 illustrates this behavior and shows that the refined modulation accounts satisfactorily for the observed modulation. Selected modulation parameters are given in Table IV.

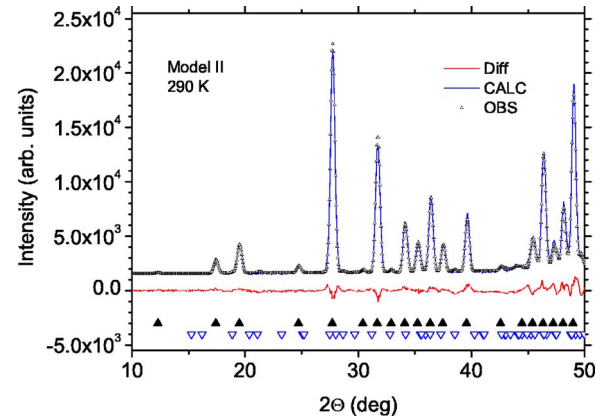


FIG. 9. (Color online) Section of the graphical result of the Rietveld refinement (Ref. 25) of SBN61 powder data collected on HRPT using the high-resolution mode, $\lambda=1.886$ Å, at temperature $T=290$ K. Modulations q_1 and q_2 have been fixed to $(0.3075, \pm 0.3075, 0)$ using a doubled c axis corresponding to $(0.3075, \pm 0.3075, 0.5)$ in the original cell. hkl 's are marked by closed triangles (average structure, upper row) and by open triangles (incommensurate satellites, lower row). Detailed refinement parameters are listed in Ref. 26, Tables VII and VIII.

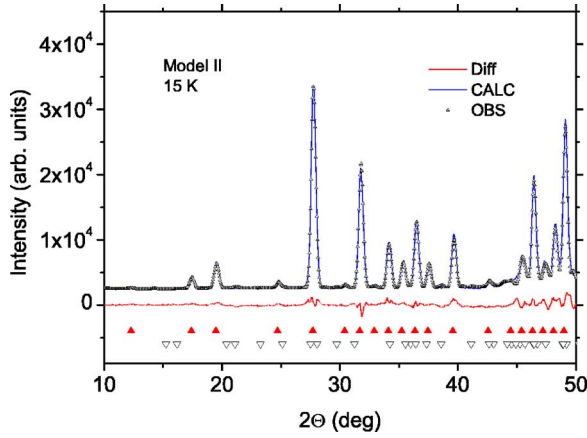


FIG. 10. (Color online) Section of the graphical result of the Rietveld refinement (Ref. 25) of SBN61 powder data collected on HRPT using the high-resolution mode, $\lambda=1.886$ Å, at temperature $T=15$ K. Modulations q_1 and q_2 have been fixed to $(0.3075, \pm 0.3075, 0)$ using a doubled c axis. hkl 's are marked by closed triangles (average structure, upper row) and by open triangles (incommensurate satellites, lower row). The refinement is clearly improved compared to the averaged structure refinement shown in Table II, model II. Detailed refinement parameters are listed in Ref. 26, Tables V and VI.

We observe small differences in the modulation between the 290 and 15 K measurements, e.g., the modulation of the O4 atom (Fig. 11) is slightly larger in the y direction at 290 K. Similar small differences are observed for other directions and atoms. Notably here the displacement parameters of the O4 and O5 atoms even increase with decreasing temperature.

Furthermore we find that the occupations of the Sr1 and Sr2 positions change slightly compared to the average structure, as the Sr1 occupation increases to 0.695(9) and that of Sr2 decreases to 0.415(4), and is hence in very good agreement with the single-crystal results.¹⁰ The complete listing of refined parameters for the 15 and 290 K data is given in Tables V–VIII in Ref. 26. Thereby $s(1,0)$ and $c(1,0)$ denote the sine and cosine parts of the harmonic wave for the modulation vector \mathbf{q}_1 and $s(0,1)$ and $c(0,1)$ those of \mathbf{q}_2 .

IV. DISCUSSION

The presented high-resolution diffraction data clearly show that there is no change in the average structure of SBN61 in the temperature range 300–15 K; in particular, no indications for a transition into a monoclinic or orthorhombic space group, as suggested in Ref. 12, could be detected. The structural data are supported by the specific heat measurements, where neither a latent heat nor a significant change in the slope of the C_p vs T curve, as found in Ref. 12, could be detected. The lattice parameter a shows the expected temperature dependence, as it increases steadily with increasing temperature. The temperature dependence of c reflects the relaxor behavior of the ferroelectric phase transition at $T_c \approx 350$ K. Notably these structural changes start already at $T=200$ K and end at about 400 K, where the parameter c increases again up to 500 K. These results are in excellent agreement with the x-ray diffraction results of Prokert *et al.*,¹³ where also the decrease in c between 200 and 450 K was observed. Hence the anisotropic thermal expansion reported by Qadri *et al.*²⁷ in the temperature range 160–300 K

TABLE III. Comparison of the averaged structures of $\text{Sr}_{0.61}\text{Ba}_{0.39}\text{Nb}_2\text{O}_6$ (model I) at 15 and 290 K.

T (K)	Atom	Occupancy	x	y	z	U_{iso}
15	Nb1	1	0	0.5	−0.0211(18)	0.0003(17)
290	Nb1	1	0	0.5	−0.0179(18)	0.0053(18)
15	Nb2	1	0.0737(2)	0.2129(2)	−0.0194(13)	0.0035(10)
290	Nb2	1	0.0736(2)	0.2127(2)	−0.0176(14)	0.0056(10)
15	Sr1	0.656(14)	0	0	0.229(3)	0.006(3)
290	Sr1	0.649(12)	0	0	0.223(3)	0.005(3)
15	Ba@Sr2	0.4875	0.1682(3)	0.6682(3)	0.2383	0.026(2)
290	Ba@Sr2	0.4875	0.1693(3)	0.6693(3)	0.2383	0.031(2)
15	Sr2	0.434(7)	0.1682	0.6682	0.2383	0.026(2)
290	Sr2	0.438(6)	0.1693	0.6693	0.2383	0.031(2)
15	O1	1	0.2174(3)	0.2826(3)	−0.0468(18)	0.0111(17)
290	O1	1	0.2169(3)	0.2831(3)	−0.0427(19)	0.0139(16)
15	O2	1	0.1386(3)	0.0679(4)	−0.0475(15)	0.0161(11)
290	O2	1	0.1389(3)	0.0670(3)	−0.0422(15)	0.0190(10)
15	O3	1	−0.0066(2)	0.3449(3)	−0.0416(13)	0.0098(11)
290	O3	1	−0.0067(2)	0.3443(3)	−0.0394(14)	0.0132(11)
15	O4	1	0.0830(4)	0.2017(3)	0.217(2)	0.0370(15)
290	O4	1	0.0814(3)	0.2031(3)	0.221(2)	0.0370(13)
15	O5	1	0	0.5	0.235(3)	0.048(4)
290	O5	1	0	0.5	0.237(3)	0.044(3)

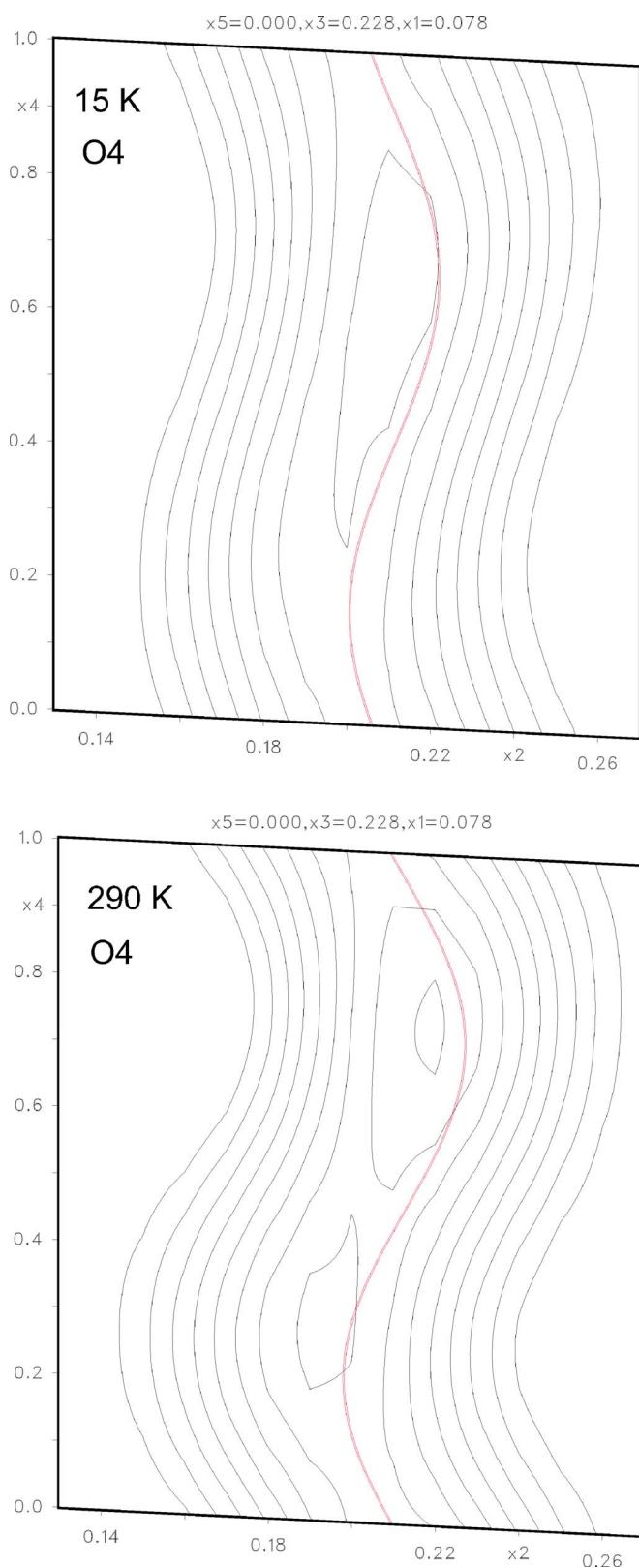


FIG. 11. (Color online) Modulation of O4 in SBN61 in the x_4 - x_2 plane at $T=15$ (top) and 290 K (bottom). The O4 atom is marked by a bold (red) line. The cut is through five-dimensional space as defined by Eqs. (2)–(4) where x_1 - x_3 is the standard reciprocal space.

TABLE IV. Comparison of the positional modulation factors (model II, Table II) for $\text{Sr}_{0.61}\text{Ba}_{0.39}\text{Nb}_2\text{O}_6$ (SBN61) measured on HRPT at SINQ at $\lambda=1.886$ Å in the high-resolution mode as tabulated in Tables V and VI for 15 K and Tables VII and VIII for 290 K in the supplementary material (Ref. 26).

Atom	Parameter	15 K	290 K
O2	$z(s,1,0)$	-0.0219(16)	-0.0148(17)
O2	$z(c,1,0)$	-0.0156(18)	-0.0100(17)
O2	$z(s,0,1)$	-0.0116(18)	-0.0057(16)
O2	$z(c,0,1)$	0.0354(12)	0.0211(14)
O3	$z(s,1,0)$	0.0161(16)	0.0297(15)
O3	$z(c,1,0)$	0.0146(15)	0.0054(16)
O3	$z(s,0,1)$	0.0174(14)	0.0188(16)
O3	$z(c,0,1)$	-0.0158(15)	-0.0171(16)
O4	$x(s,1,0)$	0.0037(14)	0.0041(12)
O4	$x(c,1,0)$	0.0243(9)	0.0251(8)
O4	$x(s,0,1)$	0.0135(13)	0.0139(13)
O4	$x(c,0,1)$	-0.0217(10)	-0.0188(10)
O4	$y(s,1,0)$	-0.0093(10)	-0.0142(9)
O4	$y(c,1,0)$	-0.0055(9)	-0.0033(9)
O4	$y(s,0,1)$	-0.0081(10)	-0.0064(10)
O4	$y(c,0,1)$	0.0085(9)	0.0094(9)
O5	$x(s,1,0)$	0.0117(12)	0.0085(13)
O5	$x(s,0,1)$	-0.0096(14)	-0.0056(15)
O4	U_{iso}	0.0104(15)	0.0078(14)
O5	U_{iso}	0.038(3)	0.0033(3)

in SBN75 can be explained completely with the onset of the relaxor phase transition at $T_c \approx 300$ K, bearing in mind that in SBN75 the phase transition temperature ($T_c \approx 300$ K) is lower than in SBN61 ($T_c \approx 350$ K) (Ref. 28) and in complete agreement with the earlier results on SBN75 of Prokert *et al.*²⁹

More insight into the origin of the transverse dielectric anomalies observed¹⁴ below 100 K might be obtained from the inspection of the modulated refinement on the two high-resolution powder patterns. The structural results obtained from our powder data at 290 K are in reasonable agreement with the single-crystal data²³ and show that the average structures are not sufficient to study the SBN system (compare Table II and Figs. 10 and 8). As illustrated for the atom O4 the positional modulation is smaller at 15 K compared to 290 K (see Fig. 11) indicating that a small change in the amplitude of the incommensurate structure occurs upon cooling. Since the modulation is mainly due to the tilting of the NbO_6 octahedra, we would expect a change in their configuration or the freezing of a possible dynamic behavior such as a temperature-driven rotation of the NbO_6 octahedra. This interpretation is in line with the argumentation of Ko *et al.*,¹⁴ who observed a temperature-driven process with an activation energy of about 0.087 eV and an attempt frequency of 1.5×10^{11} Hz (Arrhenius-like). Effectively a distribution of relaxation times was observed leading to a distribution of activation energies in the range 0.08–0.22 eV, which might be explained by random environments of the oxygen octahe-

dra due to the incommensurate structure. This explanation might also hold for the interpretation of the Raman data, as the authors of the Raman study stated that a change in the local symmetry of the NbO_6 octahedra would also explain their observations.¹⁵ Ko and Kojima performed also low-temperature Brillouin spectroscopy on SBN61 and found that the coupling between the acoustic modes and the thermal activation process is very weak.³⁰ The observed mild softening in the temperature dependence of the frequency shifts of the acoustic modes was ascribed to a dynamical behavior rather than a structural phase transition. More detailed information about a possible phonon softening at low temperatures might be obtained from inelastic neutron measurements, which to our knowledge have not been performed so far. The specific heat data can also be interpreted in terms of freezing in of some dynamics. The fact that the specific heat of SBN61 cannot be explained by a simple Debye βT^3 dependence was already observed in 1982 by Henning and co-workers,³¹ which explained their findings in the temperature range 0.3–30 K with a glasslike behavior. Note that this glassy behavior in the specific heat was used by De Yoreo *et al.* to separate ferroelectrics into two classes.³² Our experiments are in good agreement with these observations, as also we have to explain the low temperature part using three Einstein modes in addition to the Debye part. The glasslike features might well be due to the freezing of a rotational dynamics of the oxygen octahedra, which then solidifies in more or less arbitrary directions at low temperatures. Such a freezing could also explain the fact that the obtained fit quality of the incommensurate modulation is worse at low temperature, since a rotational dynamics at high temperature leads only to the smearing out of displacement parameters, while a frozen configuration at low temperature might considerably disturb the periodicity of the modulation. The harmonic approximation used for the description of the incommensurate modulation cannot account for such a distortion. However, an indication for an oxygen octahedra distortion

are the rather large displacement parameters for the atoms O4 and O5 at 15 K. A further hint to dynamical behavior is the intrinsic broadness of the satellite peaks as observed in single crystal neutron diffraction at room temperature.^{22,23} However, the reason for this broadening is unknown at the moment, and a temperature-dependent investigation has to show whether it vanishes at low temperatures, as indicated by the lower quality in the fit shown in Table II.

V. CONCLUSIONS

Neutron powder diffraction experiments show no structural phase transition of the average structure of SBN61. They give evidence that the dielectric anomalies observed below $T=100$ K are due to small changes in the amplitude of the incommensurate modulation of the oxygen octahedra, and hence support the interpretation of Ko *et al.*,¹⁴ that some barrier crossing processes such as the concerted rotation of the oxygen octahedra are responsible for the observed dielectric phenomena. This interpretation is supported by specific heat measurements, which exhibit glasslike features at low temperatures. Furthermore we showed that the structural changes connected with the high-temperature ferroelectric phase transition ($T_c \approx 350$ K) start already at about 200 K and are responsible for the anisotropic thermal expansion in SBN crystals²⁷ in this temperature range.

ACKNOWLEDGMENTS

Neutron beam time at the high-resolution powder diffractometers HRPT and POLDI at the Swiss Spallation Neutron Source (SINQ) is gratefully acknowledged, as well as the support by the LDM group of PSI and the crystal growth department of the University of Osnabrück. The development of the JANA2000 program package was supported by the Grant Agency of the Czech Republic, Grant No. 202/06/0757.

*Electronic address: jurg.schefer@psi.ch

¹A. Glass, *J. Appl. Phys.* **40**, 4699 (1969).

²M. Ewbanks, R. Neurgaonka, and W. Cory, *J. Appl. Phys.* **62**, 374 (1987).

³T. Woike, U. Dörfler, L. Tsankov, G. Weckwerth, D. Wolf, M. Wöhlecke, T. Granzow, R. Pankrath, M. Imlau, and W. Kleemann, *Appl. Phys. B: Lasers Opt.* **72**, 661 (2001).

⁴A. S. Bhalla, R. Guo, L. E. Cross, G. Burns, F. H. Dacol, and R. R. Neurgaonkar, *Phys. Rev. B* **36**, 2030 (1987).

⁵J. Dec, W. Kleemann, V. Bobnar, Z. Kutnjak, A. Levstik, R. Pirc, and R. Pankrath, *Europhys. Lett.* **55**, 781 (2001).

⁶T. Granzow, T. Woike, M. Wöhlecke, M. Imlau, and W. Kleemann, *Phys. Rev. Lett.* **92**, 065701 (2004).

⁷W. Kleemann, *J. Mater. Sci.* **41**, 129 (2006).

⁸J. Schneck, J. Toledano, R. Whatmore, and F. Ainger, *Ferroelectrics* **36**, 327 (1981).

⁹A. Balagurov, F. Prokert, and B. Savenko, *Phys. Status Solidi A* **103**, 131 (1987).

¹⁰T. Woike, V. Petříček, M. Dusek, N. Hansen, P. Fertey, C. Lecomte, A. Arakcheeva, G. Chapuis, M. Imlau, and R. Pankrath, *Acta Crystallogr., Sect. B: Struct. Sci.* **59**, 28 (2003).

¹¹S. Chernaya, B. Maksimov, L. A. Verin, I. V. and. Ivleva, and V. Simonov, *Crystallogr. Rep.* **42**, 375 (1997).

¹²Y. Xu, Z. Li, W. Li, H. Wang, and H. Chen, *Phys. Rev. B* **40**, 11902 (1989).

¹³F. Prokert, J. Ihringer, and H. Ritter, *Ferroelectr., Lett. Sect.* **20**, 73 (1995).

¹⁴J.-H. Ko, S. Kojima, S. G. Lushnikov, R. S. Katiyar, T.-H. Kim, and J.-H. Ro, *J. Appl. Phys.* **92**, 1536 (2002).

¹⁵J. L. B. Faria, P. T. C. Freire, A. P. Ayala, F. E. A. Melo, J. Mendes Filho, C. W. A. Paschoal, I. A. Santos, and J. A. Eiras, *J. Raman Spectrosc.* **34**, 826 (2003).

¹⁶E. Buixaderas, M. Savinov, M. Kempa, S. Veljko, S. Kamba, J. Petzelt, R. Pankrath, and S. Kapphan, *J. Phys.: Condens. Matter* **17**, 653 (2005).

¹⁷J. Schefer, M. Koennecke, A. Murasik, A. Czopnik, T. Straessle,

- P. Keller, and N. Schlumpf, *Physica B* **276–278**, 146 (2000).
- ¹⁸W. E. Fischer, *Physica B* **234–236**, 1202 (1997).
- ¹⁹U. Stuhr, H. Spitzer, J. Egger, A. Hofer, P. Rasmussen, D. Graf, A. Bollhalder, M. Schild, G. Bauer, and W. Wagner, *Nucl. Instrum. Methods Phys. Res. A* **545**, 330 (2005).
- ²⁰U. Stuhr, *Nucl. Instrum. Methods Phys. Res. A* **545**, 319 (2005).
- ²¹S. Podlozhenov, J. Graetsch, H. A. Scheider, M. Ulex, M. Wöhlecke, and K. Betzler, *Acta Crystallogr., Sect. B: Struct. Sci.* (to be published).
- ²²D. Schaniel, J. Schefer, V. Petříček, M. Imlau, T. Granzow, and T. Woike, *Appl. Phys. A: Mater. Sci. Process.* **74**, S963 (2002).
- ²³D. Schaniel, Thesis, ETH Zurich, 2003, <http://e-collection.ethbib.ethz.ch/>
- ²⁴P. Wolff, T. Janssen, and A. Janner, *Acta Crystallogr., Sect. A: Cryst. Phys., Diffr., Theor. Gen. Crystallogr.* **37**, 625 (1981).
- ²⁵V. Petříček, M. Dušek, and L. Palatinus, Computer code JANA2000 (Institute of Physics, Praha, 2000).
- ²⁶See EPAPS Document No. E-PRBMDO-74-010637 for supplementary materials about $\text{Sr}_{0.61}\text{Ba}_{0.39}\text{Nb}_2\text{O}_6$. This document can be reached via a direct link in the online article's HTML reference section or via the EPAPS homepage (<http://www.aip.org/pubservs/epaps.html>).
- ²⁷S. B. Qadri, J. A. Bellotti, and D. H. Wu, *Appl. Phys. Lett.* **86**, 251914 (2006).
- ²⁸C. David, T. Granzow, A. Tunyagi, M. Wöhlecke, T. Woike, K. Betzler, M. Ulex, M. Imlau, and R. Pankrath, *Phys. Status Solidi A* **201**, R49 (2004).
- ²⁹F. Prokert, J. Ihringer, and H. Ritter, *Ferroelectr., Lett. Sect.* **24**, 1 (1998).
- ³⁰J.-H. Ko, and S. Kojima, *J. Korean Phys. Soc.* **41**, 241 (2002).
- ³¹I. Henning, M. Mertig, R. Plath, G. Pompe, E. Hegenbarth, and R. Schalge, *Phys. Status Solidi A* **73**, K105 (1982).
- ³²J. J. De Yoreo, R. O. Pohl, and G. Burns, *Phys. Rev. B* **32**, 5780 (1985).
- ³³A. Yamamoto, *Acta Crystallogr., Sect. A: Found. Crystallogr.* **52**, 509 (1996).